Hydrol. Earth Syst. Sci. Discuss., 5, 2373–2407, 2008
www.hydrol-earth-syst-sci-discuss.net/5/2373/2008/
© Author(s) 2008. This work is distributed under
the Creative Commons Attribution 3.0 License.

Hydrology and Earth System Sciences Discussions

Papers published in *Hydrology and Earth System Sciences Discussions* are under open-access review for the journal *Hydrology and Earth System Sciences*

Significance of tree roots for preferential infiltration in stagnic soils

B. Lange[1,2], **P. Luescher**[1], **and P. F. Germann**[2]

[1]Swiss Federal Institute for Forest, Snow and Landscape Research, Zuercherstrasse 111, 8903 Birmensdorf, Switzerland
[2]Soil Science Section, Department of Geography, University of Bern, Hallerstrasse 12, 3012 Bern, Switzerland

Received: 21 July 2008 – Accepted: 21 July 2008 – Published: 26 August 2008

Correspondence to: B. Lange (benjamin.lange@wsl.ch)

Published by Copernicus Publications on behalf of the European Geosciences Union.

Abstract

It is generally believed that roots have an effect on infiltration. In this study we analysed the influence of tree roots from Norway spruce (*Picea abies* (L.) Karst), silver fir (*Abies alba* Miller) and European beech (*Fagus sylvatica* L.) on preferential infiltration in stagnic soils in the northern pre-Alps in Switzerland. We conducted irrigation experiments (1 m^2) and recorded water content variations with time domain reflectrometry (TDR). A rivulet approach was applied to characterise preferential infiltration. Roots were sampled down to a depth of 0.5 to 1 m at the same position where the TDR-probes had been inserted and digitally measured. The basic properties of preferential infiltration, film thickness of mobile water and the contact length between soil and mobile water in the horizontal plane are closely related to fine root densities. An increase in root density resulted in an increase in contact length, but a decrease in film thickness. We modelled water content waves based on fine root densities and identified a range of root densities that lead to a maximum volume flux density and infiltration capacity. These findings provide convincing evidence that tree roots improve soil structure and thus infiltration.

1 Introduction

The impact of forests on reducing surface runoff has been a subject of study in Europe for over 100 y (e.g. Demonzey, 1878; Engler 1919). It has been addressed on various spatial scales, especially with regard to the effect of clear cutting on peak flow (e.g. Beschta et al., 2000; Cheng et al., 2001; Tremblay et al., 2008). For example, Cognard-Plancq et al. (2001) claimed that forest-covered soils can store more water than soils without trees. Water storage depends not only on the percentage of forested area, but also on the forest site in a catchment area, as different sites influence infiltration capacities differently (Badoux et al., 2006).

Macropores, which are large continuous openings formed by soil fauna, freeze/thaw cycles, shrinking processes, subsurface erosion or plant roots (Beven and Germann,

1982), are assumed to increase infiltration rates and thus preferential flow (Mapa, 1995). Preferential flow is characterised by a non homogenous movement of water through soils (Gish et al., 1998). Three main types of preferential infiltration have been identified: bypass flow (Beven and Germann, 1982; Bouma, 1991), finger flow in structureless, sandy soils (e.g. Kawamoto et al., 2004), and funnel flow (Kung, 1990). To describe preferential flow in structured soils, various models of preferential infiltration have been proposed since Richards' equation (1931) and Darcy's law (1856) are inadequate (Gerke, 2006). Under conditions of near saturation, preferential flow has been described in two different ways (Germann et al., 2007). The first is to approach the expected preferential flow from Richards' domain. Gärdenäs et al. (2006), for example, applied Richards' equation to four approaches, including one equilibrium and three non-equilibrium approaches, and implemented them in the HYDRUS-2D two-dimensional transport model.

The second way deduces preferential flow from free-surface flow. Germann and Beven (1985) approached preferential flow using kinematic wave theory, including a sink function for macropore flow to take account of sorption by the surrounding matrix. Many authors have adapted the kinematic wave approach. Di Pietro et al. (2003), for example, described preferential flow by a travelling-dispersive wave, which yields a linear solution of a non-linear convective-dispersive equation. German et al. (2007) proposed a rivulet approach to preferential infiltration. The approach is based on the assumption that gravity is the only flow-driving force and viscosity is the only force that opposes gravity. Tiny water streaks, termed rivulets, are the basic units of preferential infiltration. Film thickness F^1 (m) and length of contact L^2 ($\mathrm{m\,m^{-2}}$) in the horizontal plane with the stationary parts are the basic properties of a rivulet. The velocities of the wetting and drainage fronts, the mobile water content and the volume flux density of drainage are linked to the rivulet's basic properties. In this paper, the rivulet approach is used to characterise preferential flow.

[1] Arithmetic mean of film thickness of mobile water (10^{-6} m).

[2] Maximal sum of contact length between mobile water and soil ($10^{3}\,\mathrm{m\,m^{-2}}$).

Although the notion that roots influence preferential flow is widespread, root parameters have seldom been recorded in relation to preferential flow. The roots of corn (*Zea mays*) and alfalfa (*Medicago sativa*) are able to form well-connected macropores that enhance preferential flow. Furthermore, the saturated hydraulic conductivity (K_{sm}) in soil columns with root channels was six time higher than in control columns without roots (Li and Ghodrati, 1994). Jøergensen et al. (2002) found that 94% of flow in a clay-rich till was conducted along root channels, while only 6% flowed along fractures without root channels. Numerous studies have visualised preferential flow paths by staining (e.g. Alaoui and Goetz, 2008; Weiler and Naef, 2003). Roots, decayed or live, appear to be the most important agents of preferential flow paths, but not all roots are necessarily associated with them (Perillo et al., 1999). However, little is known about the relation between root morphology and preferential infiltration. The objective of this study is, therefore, to identify the impact of tree roots on preferential flow according to the rivulet approach (Germann et al., 2007).

2 Theory

Infiltration at the surface is considered a rectangular pulse of duration T_S (s) and volume flux density q_S($\mathrm{m\,s^{-1}}$). It releases a water content wave (wcw) at the beginning of water input at time t=0 (s). A rivulet is the basic unit of a wcw. It is a tiny streak of water that is gravity-driven and viscosity-controlled. It is, however, too tiny to be measured in situ with ordinarily applied instrumentation, such as TDR- equipment. All the rivulets moving with the same velocity are summarized as a rivulet ensemble whose mobile water content is measurable in situ. Superposition of all rivulet ensembles adds up to the entire wcw. A rivulet ensemble consists of a water film that is defined with its thickness F (m) and length of contact L ($\mathrm{m\,m^{-2}}$) per A ($\mathrm{m^2}$) of the ensemble with the stationary parts of the soil-water system, where A is the cross-sectional area of soil. The j^{th} ensemble's wetting and draining fronts arrive at depth Z at times $t_W(Z)_j$ and $t_D(Z)_j$, where $1 \le j \le N_{RE}$. The following expressions quantify flow. The mobile water

content of a rivulet ensemble, w, is

$$w = L \cdot F \tag{1}$$

($m^3\,m^{-3}$), the average velocity of the film, v, is

$$v = \frac{g}{3 \cdot \eta} F^2, \tag{2}$$

($m\,s^{-1}$), where g (=9.81 $m\,s^{-2}$) is acceleration due to gravity and η (=$10^{-6}\,m^2\ s^{-1}$) is kinematic viscosity of water.

An ensemble's volume flux density, q, is given as

$$q = w \cdot v = \frac{g}{3 \cdot \eta} F^3 \cdot L \tag{3}$$

Knowing any two of the three Eqs. (1) to (3) suffices to define an ensemble's F and L, and subsequently the third expression. Germann et al. (2007) provide the details. The arrival time of an ensemble's wetting front, t_w, at a depth Z (m) is

$$t_w(Z) = \frac{Z}{v_W} = \frac{Z}{F^2} \frac{3\eta}{g}. \tag{4}$$

The combination of Eqs. (2) and (4) leads to the j^{th} ensemble's film thickness F_j

$$F_j = \frac{1}{\sqrt{t_{W,j}(Z)}} \sqrt{\frac{3Z\eta}{g}} = \sqrt{\frac{3\upsilon_{w,j}\eta}{g}}, \tag{5}$$

and the combination of Eqs. (1) and (5) results in the ensemble's contact length, L, with stationary parts per A being expressed as

$$L = w \sqrt{\frac{t_W(Z)g}{3Z\eta}}. \tag{6}$$

A wcw is composed of N_{RE} rivulet ensembles. The sum of contact lengths, SL, per A is

$$SL = \sum_{j=1}^{N_{RE}} L_j. \tag{7}$$

Superimposing the trailing waves of N_{RE} rivulet ensembles results in the wcw's trailing wave at depth Z as

$$\omega_{en}(Z,t) = (t - T_S)^{-1/2} \sum_{j=1}^{N_{RE}} (L_j F_j) \left[t_D(Z)_j - T_s\right]^{1/2} = (t - T_s)^{-1/2} \sum_{j=1}^{N_{RE}} (w_{R_j}) \left[t_D(Z)_j - T_s\right]^{1/2}, \tag{8}$$

where $t_D(Z)j$ (s) is the arrival time of the draining front at depth Z of the j^{th} ensemble, i.e.,

$$t_D(Z)_j = T_S + \frac{t_W(Z)_j}{3}. \tag{9}$$

Interpretation of a time series $\theta(Z,t)$ (Figs. 1 and 3) is according to the following 9-point protocol adapted from Germann et al. (2007):

1. Determine θ_F, Fig. 1.
2. Subtract θ_F from $\theta(Z,t)$, which yields $w(Z,t)$.
3. Partition the increasing limb of $w(Z,t)$ into N_R=10 rivulet ensembles, yielding w_j, Eq. (1).
4. Assign arrival times of the wetting fronts, $t_W(Z)_j$, to each rivulet ensemble (Fig. 2).
5. Calculate arrival times of the draining fronts, $t_D(Z)_j$, for each rivulet ensemble, Eq. (9).

6. From the arrival times of the wetting fronts obtain the film thickness, F_j, Eq. (5), and
7. the contact length per area, L_j, Eq. (6).
8. Calculate the trailing wave of the wcw according to Eq. (8).
9. Determine the volumetric flux density of each rivulet ensemble, q_j, Eq. (3).

Figure 2 illustrates the procedure with N_{RE}=3. For our analysis, N_{RE} was determined as 10 (according to Germann et al., 2007). Figure 3 shows the application of the rivulet approach to the measured wcw. The comparison of the performance of Eq. (8) with the data of the trailing wave of a wcw gives an independent measure of the adequacy of the rivulet approach. The coefficient of determination between approach and data in Fig. 3 was R^2=0.983.

3 Site, materials and methods

3.1 Site and soil description

The study area is located near Rueschegg in Canton Bern in the northern pre-Alps in Switzerland (46°46′N, 7°23′E, 1000 m a.s.l.). Annual mean precipitation is approximately 1600 mm. The bedrock consists of Flysch, a sediment of the tertiary, composed of marled clays interlaced with stony or sandy layers. The stand is classified as a Bazzanio-Abietetum (Ellenberg and Klötzli, 1972) with Norway spruce (*Picea abies*(L.) Karst.) as the most abundant species mixed with silver fir (*Abies alba* Miller) and a few solitary European beech (*Fagus sylvatica* L.). Whortleberry (*Vaccinium myrtillus*) dominates the herb and shrub layer.

The region where the study was conducted has been frequently affected by floods in the last twenty years (1990, 2005 and 2007, Federal Office for the Environment, 2008), due to high levels of precipitation and the hydromorphic soils. The soils are classified as

Gleys, Cambisols and gleyic or stagnic Cambisols, according to FAO-Unesco (1994). Local ridges and depressions characterise the micro-topography on a scale of 1 to 10 m. Hydromorphic characteristics occur below a depth of 3 to 35 cm, depending on the micro-topography. As a consequence, the maximum root depths, especially those of spruce and beech, are limited. Thirteen plots were investigated. They differ with respect to the species, tree diameters and the distances between the tree trunks and the plots. Table 1 lists the attributes of each plot. The slopes of the plots are between 0 and 14°.

Soil properties were determined from samples dried for 48 h at 100°C for density and at 60°C for pH and texture. Three cylinders per horizon 1000 cm^3 in volume and 10 cm in height were used to calculate the bulk density. Porosity was calculated from the bulk density, assuming a particle density of 2650 $kg\,m^{-3}$. The particle-size distribution separation was obtained with the pipette method. Table 1 lists the soil properties. The pH ($CaCl_2$) varies between 2.8 and 6.6 in the topsoil and between 3.1 and 7.5 in the mineral layer. Bulk densities vary from 0.19 to 1.01 $Mg\,m^{-3}$ in the organic and Ah-horizons and from 1.21 to 1.43 $Mg\,m^{-3}$ in the subsoil. Thus, root growth is not limited by soil compaction. The particle size distributions vary over a considerable range. The Ah-horizons consist of loam, clay loam, sandy loam or sandy clay loam, and the mineral horizons of loam, sandy clay loam, sandy clay or clay according to Soil survey division staff (1993).

The basic units for the investigation were the morphological horizons. The root morphology and the chemical, physical, and hydrological parameters refer to the morphological horizons. There was a data set available for each horizon, consisting of water content measurements, root morphology and the physical and chemical soil parameters.

3.2 Instrumentation and infiltration experiments

Soil moisture was measured with TDR probes. The wave guides consisted of two paired, 0.15 m long stainless steel rods, 30 mm apart and 5 mm in diameter. The rods

were electrically connected with a 50Ω coax cable to a SDMX 50 coaxial multiplexer that was controlled by a CR10X micro logger. The electrical pulses were generated by a Campell TDR100 device which also received the signals. The measurement interval was set to 60 s. We applied the transfer function of Roth et al. (1990) to calculate the volumetric water content. Prior to the installation, the TDR probes were calibrated by submerging each wave-guide. The corresponding dielectric number was set equal to the volumetric water content of 1 $m^3 m^{-3}$. For the installation of the wave-guides, soil profiles were excavated. The TDR-probes were installed horizontally at the centre of each horizon.

The rain simulator consisted of a metallic disc (1 m×1 m) that was perforated with 100 holes attached to small tubes with inner diameters of 2 mm that led to a reservoir. The tubes were mounted in a 0.1×0.1 m square pattern. During irrigation, a motor moved the disc backwards and forwards ±50 mm in both horizontal dimensions so that it took approximately 1800 s until a tube reached exactly the same position. The intensity of the irrigation was controlled by a flow meter. The distances between the metallic disc and the soil surface were between 0.3 and 0.5 m. During the experiment, the 1 m^2 irrigated area was covered with a waterproof 3×3 m tent in order to protect the setup and the soil from precipitation.

Each plot was irrigated three times for one hour at approximately 23 h intervals. The volume flux density of irrigation was 70 mm/h, which is the annual hourly maximum for this region with return periods between 150 and 200 y. The rates never resulted in surface runoff.

3.3 Root morphology

Each plot was sampled after irrigation with soil cores 5 cm away from the profile face, exactly in the same place where the TDR probes had been installed. Soil cores were taken with a HUMAX soil corer (diameter 10 cm) to depths between 0.5 and 1 m, depending on the location of the lowest TDR probe. The probes consisted of 25 cm long segments in plastic tubes. The soil was left undisturbed during sampling and storage

(in a refrigerator at 4°C for no longer than 12 weeks). Each core segment was separated along the boundaries of the horizons into different layers that were analyzed separately.

The roots were sieved and washed in a 1 mm sieve with tap water. All root fragments (woody and herb roots) were collected and stored at 4°C. Root morphology was analyzed with WinRHIZO (V4.1c; Regent Instruments Inc., Quebec, Canada). We recorded root length (cm), surface area (cm^2), diameter (cm) and volume (cm^3). Each parameter was calculated for the total root sample and for fine (Ø≤2 mm) and coarse roots (Ø>2 mm) separately. Finally, the fine and coarse roots were dried for 48 h at 60°C and subsequently weighed.

4 Results

4.1 Hydrological parameters

A total of 225 water content waves, wcw, from 75 horizons were recorded with the TDR-equipment. The coefficient of determination, R^2, between measured and modelled wcw exceeded 0.70 in only 21 horizons (49 water content waves), where we assume preferential infiltration according to Eqs. (1) to (9). The remaining 54 horizons showed perched water tables due to the impermeable soil layers, which contradict the conditions of rivulet flow. Since the aim of this study was to explore the relevance of tree roots for preferential infiltration, we included only the 49 water content waves in the further analyses.

Each of the 21 horizons showed a coefficient of determination $R^2 \geq 0.70$ between measured and modelled wcw during two or three of the three irrigations. For each horizon we considered the wcw with the best correlation between measured and calculated trailing waves (according to Eq. 8), which resulted in a data base consisting of the root morphology and associated soil moisture recordings from 13 different soil profiles and of 21 morphological horizons.

Table 2 lists the key points in the measured time series of volumetric water content $\theta(Z,t)$. The arithmetic mean of the 21 amplitudes of the drainage, w_s, was 0.072 $m^3\,m^{-3}$ ranging between 0.021 and 0.143 $m^3\,m^{-3}$.

The velocity of a wetting front follows from

$$\upsilon_w = \frac{Z}{t_w} \tag{10}$$

The velocities were between 0.11 and 1.11 $mm\,s^{-1}$ and compare well with those measured by Germann et al. (2006), which were between 0.1 and 5.5 $mm\,s^{-1}$. Volume flux density q, according to Eq. (3), was between 1.69 and 31.8×10^{-6} $m\,s^{-1}$.

Adoption of Eq. (5) produced an estimate of the rivulet's film thickness. The arithmetic mean of the ten film thicknesses, which formed the increasing limb of the soil moisture wave (Fig. 3), is the wave's overall film thickness F. The thinnest film was 4.2, and the thickest 18.1 μm. The maximum sum of the contact lengths SL, according to Eq. (7), varied between 1448 and 25 116 $m\,m^{-2}$ for the 21 wcws.

4.2 Root morphology

Root morphology was determined in each morphological horizon that produced a wcw. The root distributions of the tree species were not distinguishable according to soil depth in terms of the lengths of the fine roots (≤2 mm) and coarse roots (>2 mm) or the total root length (one way ANOVA, $P<0.05$). The median fine root length per soil volume (0.064 $cm\,cm^3$), including all species and soil depths, was one order of magnitude higher than the median length of coarse roots (0.005 $cm\,cm^{-3}$).

Figure 4 gives an overview of root lengths per soil volume.

The variation in fine root length per soil volume (FRL[3]) was considerable, exhibiting values between 0.017 and 1.852 $cm\,cm^{-3}$. The FRL of spruce, fir and beech reached the maximum lengths in topsoil with roots from the root diameter classes of 0.5–1

[3]Fine root length per soil volume ($cm\,cm^{-3}$).

and 1–1.5 mm (Fig. 4). The arithmetic means of root surface areas per soil volume (RA[4]) did not significantly differ (one way ANOVA, $P<0.05$, not shown) according to species. The main part of the RA was formed by fine roots, even though the differences appeared less distinct in comparison to RL[5]. The median of the fine root surface area (0.020 $cm^2\,cm^{-3}$), including all species and age classes, exceeded the coarse roots' surface area (0.007 $cm^2\,cm^{-3}$) by a factor of approximately three. Maximum values of RA were found within the diameter class of 0.5–1 mm. Compared to RL, the peak of RA tended to flatten in higher diameter classes.

4.3 Fine root density and hydrological parameters

For all tree species fine roots formed the main part of the complete root system. Therefore only the morphology of fine roots was considered in further analysis. Our analyses revealed few correlations between the fine root properties and the parameters of the mobile water in the soil. Pearson product-moment analysis identified four groups where the correlations were significant ($P<0.05$).

The first group shows the effect of the soil depth on F, L, bulk density and root morphology. With increasing soil depth, bulk density increased and the films of mobile water became thicker, while L and the length, surface area and volume of fine roots decreased. The second group, the key points of the wcws, initial volumetric soil moisture θ_{in}, maximum volumetric soil moisture θ_{max} and the water content after the drainage θ_F were closely correlated with each other. In particular θ_{in} vs. θ_F exhibited a coefficient of correlation of $r=0.989$. The amplitude of drainage, w_s, was strongly affected by L ($r=0.925$) and, to a minor degree, by F ($r=-0.571$). Furthermore, an increasing fine root density resulted in an intensification of the drainage.

[4]Total root surface area per soil volume ($cm^2\,cm^{-3}$).

[5]Total root length per soil volume ($cm\,cm^{-3}$).

The largest group of parameters has to do with root morphology (FRL, FRA[6], FRV[7]), but the group also contains the maximum sum of contact lengths L and the film thickness F of mobile water. The length, surface area and volume of fine roots were all closely correlated with each other ($0.870 \leq r \leq 0.973$). Furthermore, the contact length L and the film thickness F were negatively correlated ($r=-0.745$). The length, surface area and volume of fine roots affected the contact length L and film thickness F of mobile water. We found a maximum correlation between L and the fine root surface area ($r=0.915$), while F was negatively affected particularly by the fine root length ($r=-0.775$). Bulk density affected root morphology, F and L, but with $0.680 \leq |r| \leq 0.738$ the interrelations were less distinct than those between root morphology and F and L. Table 3 presents the relationships between fine root morphology and preferential flow factors.

According to Eq. (2), v_w should strongly relate with F. Since we applied the arithmetic mean of the $N_{RE}=10$ rivulet's film thicknesses as quantity for the film thickness of a wcw, the correlation between F and v_w was only $r=0.787$, while the correlation between v_w and the thickness of the first rivulet ensemble, which determines t_w and hence v_w, was $r=0.973$.

The fine root lengths per soil volume of the 21 horizons were classified by applying a hierarchical cluster analysis (complete linkage, Euclidean distance). We determined the boundary among the groups at an Euclidian distance of 0.75. That led to three clear clusters of FRL, which represent approximately the topsoil, the non-hydromorphic subsoil horizons and the hydromorphic subsoil layers (Fig. 5). The first group with 12 elements and the lowest root densities (FRL 0.017–0.411 $\mathrm{cm\,cm^{-3}}$, arithmetic mean 0.21 $\mathrm{cm\,cm^{-3}}$) consisted of hydromorphic subsoil layers, with the exception of ID# 13, 14, 17 and 18, which were described as unaffected by stagnic or gleyic characteristics. Group two (FRL 0.574–1.066 $\mathrm{cm\,cm^{-3}}$, arithmetic mean 0.81 $\mathrm{cm\,cm^{-3}}$) included

[6]Fine root surface area per soil volume ($\mathrm{cm^2\,cm^{-3}}$).

[7]Fine root volume per soil volume ($\mathrm{cm^3\,cm^{-3}}$).

non-hydromorphic subsoil horizons (ID# 1, 9) as well as topsoil layers (ID# 2, 5) and organic overlay (ID# 3). The third group (FRL 1.361–1.852 $\mathrm{cm\,cm^{-3}}$, arithmetic mean 1.61 $\mathrm{cm\,cm^{-3}}$) was made up of topsoil layers without any hydromorphic properties (ID# 8, 12, 19) and one Oe/Oi horizon (ID# 15).

The volumetric water content parameters θ_{in}, $\theta_{\max}$ and θ_F, the volume flux density and velocities of wetting front (v_w) did not differ among the three FRL-groups. The average soil depth of FRL-group 1 was significantly higher than that of groups 2 and 3, while between groups 2 and 3 no statistical difference was verifiable although the soil depth in the second group was almost twice as much as in the third group. Regarding bulk density, there was a slight decrease from FRL-group 1 to FRL-group 3, but only groups 1–2 and 1–3 were significantly different. The morphological properties of the fine roots were different in the three FRL-groups. Both the surface areas and the volumes of fine roots increased with increasing root length ($P<0.05$). The only exception was the fine root volumes in the second and third group that was not significantly affected by fine root length, even though the average FRV in group 3 was nearly twice that in group 2.

The preferential flow parameters L and F discriminated between the three groups. Contact length L increased from FRL-group 1 to 3. The L of group 1 achieved only 25 to 35% of the contact lengths of group 2 and 3. Film thickness behaved inversely to the contact length: with increasing fine root length, F decreased. Only the differences between groups 1 and 3 were significant at $P<0.05$ (groups 1–2 differed significantly at $P<0.1$). The difference between $\theta_{\max}$ and θ_F, w_s, rose with increasing FRL. Significant differences in the mean values of w_s were detected among FRL-groups 1–3, while the w_s of 1–2 and 2–3 were not distinguishable from each other. Figure 6 shows the varieties of soil, root and preferential flow properties among the three FRL-groups.

As Table 3 and Fig. 6 demonstrate, the fine root length FRL, contact length L and film thickness F are related to each other. Figure 7 illustrates this relation. Table 3 shows that the coefficients of correlation, r, between FRL and L, and between FRL and F exceeded 0.75 with a significance level of $P<0.001$. The regression equations

between L and FRL, and between F and FRL respectively are given by

$$F = -5.3893\,\mathrm{FRL} + 12.561 \quad (11)$$

$$L = 11.454\,\mathrm{FRL} + 1.6794 \quad (12)$$

The contact length L increases with increasing fine root length per soil volume and film thickness F decreases. The subsoil layers (group 1, Fig. 5) are characterised by low fine root densities, short contact lengths and considerable film thicknesses. By contrast, the non-hydromorphic topsoil horizons (group 3) exhibit the highest values of fine root lengths and contact lengths, but the smallest film thicknesses. Group 2 is positioned between groups 1 and 3 with intermediate fine root lengths, contact lengths and film thicknesses.

5 Applications

Film thickness and contact length are basic parameters of rivulet flow, while volume flux density, mobile water content and velocities of drainage and wetting fronts (Eqs. 1 to 9) are related to F and L. Contact length and film thickness are significantly related to fine root density (Fig. 7). Thus preferential infiltration can be modelled using fine root densities as a base. L and F are estimated with FRL, applying the equations of the regression lines between FRL and L and F, respectively (Eqs. 11 and 12). Input data for our model were fine root densities, while output data were the corresponding water content waves and therefore $\theta_{\max}$, θ_F, volume flux densities q, velocities of water and drainage fronts as well as w_s. For our example, we modelled five water content waves based on fine root densities of 0.25, 0.5, 1, 1.5, and 1.75 cm per cm^3 soil. We assume in what follows that all rivulet ensembles move with the same velocity, and that the modelled wcw moves with a sharp wetting-shock front. Table 4 shows the resulting F, L, w_s, v_W and q.

The parameters of the modelled water content waves were defined as follows: duration of irrigation (70 mm/h) was 3600 s, starting at $t=0$. The contact length of the rivulets corresponds to the maximum sum of contact lengths L (Eq. 12) of the associated fine root densities. The film thicknesses of the rivulets were determined according to Eq. (11) (arithmetic mean of film thickness). Adaptation of Eq.(1) led to the water content of the rivulet. The arrival time of the wetting front (t_w) at a depth of 0.15 m follows from Eq. (4), while Eq. (9) yields the arrival time of the drainage front. The water content waves were modelled with a time resolution of 100 s, starting at −800 and ending at 75 000 s. The application of Eq. (8) led to the trailing waves. Figure 8 shows the modelled wcws.

The pathways of the five water content curves vary, especially with regard to the maximum water content $\theta_{\max}$ ($0.052 \le \theta_{\max} \le 0.101$). A fine root density of 1 to 1.5 cm cm^{-3} resulted in the maximum content of mobile water. The amplitude of the drainage w_s is maximal at a FRL of 1.0 to 1.5 cm cm^{-3}. If the root densities were higher or lower, the amplitude of the drainage was reduced by 22 to 48%. The lowest value of $\theta_{\max}$ and therefore of w_s was reached at a root density of 0.25 cm cm^{-3}. θ_F increased with increasing FRL, but with $0.002 \le \theta_F \le 0.010$, the differences fall below 1% water content.

The volume flux density q, determined by Eq. (3), exhibits its maximum value at lower root densities (0.5 cm cm^{-3}) than the mobile water content parameters $\theta_{\max}$ and θ_F (1.25 cm cm^{-3}). Above a root density of 0.5 cm cm^{-3}, q decreased. The peak value exceeded the minimum volume flux density by a factor of about 5. F decreased with increasing FRL, so that v_w decreased with increasing FRL (Table 4). Figure 9 serves to illustrate the hydrological properties of the modelled wcws with different fine root densities.

Assuming a constant fine root density over a soil depth of 0.5 m, the minimum potential water storage capacity can be calculated taking the amplitude of drainage (w_s) as a base. After 20 h of drainage, a fine root density of 0.25 cm cm^{-3} soil leads to a potential minimum water storage capacity of 25 mm, and a FRL of 1 cm cm^{-3} to 49 mm.

As a result, the soil with the higher root density should be able to store the amount

of water of a one hour heavy precipitation with a return period of 100 y, while the site with a quarter of the fine root density could store approximately only the water of a one hour heavy precipitation with a 2-y return period.

6 Discussion

The aim of this work was to identify the impact of tree roots on preferential infiltration. Perillo et al. (1999) maintained that tree roots, both decayed and alive, appeared to be the most important initiators for preferential flow path, but they pointed out that not all roots were necessarily associated with preferential flow paths. These findings are also consistent with our results, where no clear relation between root density and the probability of the appearance of preferential flow could be found. The missing coherence may be due to the large number of parameters involved in infiltration, such as water content (Germann et al., 2007), hydrophobicity (Wang et al., 2000), open burrows and horizon boundaries (Perillo et al., 1999).

Our results support the hypothesis that tree roots are a key factor in preferential infiltration in gleyic soils with stagnic properties. We showed that the sum of contact lengths L, and to a lesser extent the arithmetic mean of film thickness F, which are the basic units of mobile water in preferential infiltration, were related to fine root densities. With increasing soil depth, and therefore bulk density, F increased and L decreased. It must be assumed that, in topsoil horizons, high root densities result in a densely branched network of pores. Thus water flows in thin films, but the contact length between the mobile water and the soil is large. This founding is also supported by Flury et al. (1994), who studied infiltration patterns using dye experiments. In their case, the uppermost 5 to 10 cm of topsoil were completely dyed. With a lower root density there are likely to be fewer pores, as it is generally accepted that roots generate macropores (e.g. Devitt and Smith, 2002). Thus the potential contact area between mobile water and soil is reduced and the film thickness of mobile water increased. This effect is aggravated at greater soil depth and bulk density, resulting in a kind of funnel effect.

Tree roots seem to particularly influence the potential contact length. Film thickness is presumedly not only determined by FRL but is also a response to the spatial distribution of pores via the soil depth and the pore geometry. The slope of the correlation line between FRL and L is approximately 2.5× grater than the correlation line between FRL and F, which indicates that an increase in FRL influences L more than F. For example, a doubling of FRL from 0.5 to 1 cm per cm^3 soil leads to a 77% increase in L, but only a 25% reduction in F. As a result, a shifting of FRL modifies L to a greater degree than F.

The application of the rivulet approach has shown that a fine root density of approximately 0.75 to 1.5 cm cm^{-3} resulted in the highest θ_{max} and w_s. Lower root densities led to a strong decrease in the contact lengths and increased film thicknesses. Above a FRL of 1.5 cm cm^{-3}, the films became so thin that the limit for the occurrence of preferential flow was achieved. Since volume flux density is a function of the product of F^3 and L, the peak value of q was reached at lower root densities ($\approx$0.5 cm cm^{-3}) than θ_{max} and w_s. To achieve maximum volume flux density and maximum drainage after the irrigation, approximately 1 cm fine roots per cm^{-3} soil appear to be the ideal fine root density. Only seven non-hydromorphic topsoil horizons of the 21 investigated layers had a root density between 0.5 and 1.5 cm cm^{-3}. Two topsoil layers exceeded this value, and 12 horizons, with the exception of one hydromorphic subsoil layer, had less than 0.5 cm roots per cm^{-3} soil.

It is impossible to specify all preferential flow paths by means of root measurements. It has been shown that cracks adjacent to living alfalfa roots have only a temporary effect, while decaying roots produce stable macropores (Mitchell et al., 1995). Noguchi et al. (1997) pointed out that at least 70% of the macropores (≥2 mm) in the topsoil and 55% in the subsoil in a forest soil in Japan were associated with roots. Hagedorn and Bundt (2002) showed that preferential flow paths in a structured forest soil persist for decades. Beven and Germann (1982) observed that macropores formed from tree roots may persist for at least 50–100 y. The turnover rates of fine roots from spruce, fir and beech were determined as approximately 0.7, 1.1 and 0.6 y^{-1}, respectively (With-

ington et al., 2006). These observations indicate how important tree roots are for the formation of preferential flow paths.

This study has contributed to understanding better the significance of tree roots on preferential flow by showing how the basic properties of preferential flow, film thickness and contact length of mobile water are influenced by the level of fine root density. We were thus able to show that tree roots improve soil structure and thus infiltrability.

7 Conclusions

We have provided evidence that fine root morphology is a key factor for infiltration. The basic properties of preferential infiltration, contact length L and film thickness F, are closely related to fine root density. We found a positive correlation between FRL and L, but a negative relation between FRL and F. This indicates that a larger fine root density does not necessarily result in an intensification of preferential infiltration.

With increasing soil depth, rivulets of preferential infiltration become thicker but the contact lengths between soil and mobile water become shorter. As a result, preferential flow in topsoil horizons is characterised by numerous thin water films, while rivulets in subsoil horizons are thicker but less frequent.

Since FRL and F and L are closely related, it was possible to model water content waves during an irrigation and subsequent drainage based on fine root densities. We showed that the rise in the water content during irrigation and subsequent fall during drainage within 20 h was at a maximum at a fine root density of approximately 1 to 1.5 cm cm^{-3}, while volume flux density q achieved its peak value at a root density of 0.5 cm cm^{-3}.

To maximise the impact of preferential flow path for flood retention in forest soils, we propose a root density of about 1 cm cm^{-3}. Our investigations have shown that a root density between 0.5 and 1.5 cm cm^{-3} was reached only in non-hydromorphic topsoil layers to a depth of approximately 20 cm. The cultivation of deep-rooting tree species improves the root density in the subsoil and therefore stimulates preferential infiltration

into deeper, hydromorphic horizons and enlarges the water-storage space.

Acknowledgements. We thank Philipp Mösch and Dieter Müller for permission to conduct our studies in their forest district and Roger Köchli for his help in the field. We are grateful to Abdallah Alaoui, Marco Carizzoni and Ingrid Hincapié from the University of Bern for their instruction in TDR-technique and the sprinkler device, and Silvia Dingwall and Barbara Lange for improving our English. This study was supported by the COST Action E38 (Woody root processes).

References

Alaoui, A. and Goetz, B.: Dye tracer and infiltration experiments to investigate macropore flow, Geoderma, 144, 279–286, 2008.

Badoux, A., Witzig, J., Germann, P. F., Kienholz, H., Lüscher, P., Weingartner, R., and Hegg, C.: Investigations on the runoff generation at the profile and plot scales, Swiss Emmental, Hydrol. Process., 20, 377–394, 2006.

Beschta, R. L., Pyles, M. R., Skaugset, A. E., and Surfleet, C. G.: Peakflow responses to forest practices in the western cascades of Oregon, USA, J. Hydrol., 233, 102–120, 2000.

Beven, K. and Germann, P.: Macropores and water flow in soils, Water Resour. Res., 18, 1311–1325, 1982.

Bouma, J.: Influence of soil macroporosity on environmental quality, Adv. Agron., 46, 1–37, 1991.

Cheng, J. D., Lin, L. L., and Lu, H. S.: Influences of forests on water flows from headwater watersheds in Taiwan, Forest Ecol. Manag., 165, 11–28, 2002.

Cognard-Plancq, A.-L., Marc, V., Didon-Lescot, J.-F., and Normand, M.: The role of forest cover on streamflow down sub-Mediterranean mountain watersheds: a modelling approach, J. Hydrol., 254, 229–243, 2001.

Demontzey, P.: Etude sur les travaux de reboisement et de gazonnement des montagnes, Imprimerie Nationale, Paris, 1878.

Devitt, D. A. and Smith, S. D.: Root channel macropores enhance downward movement of water in a Mojave Desert ecosystem, J. Arid Environ., 50, 99–108, 2002.

Di Pietro, L., Ruy, S., and Capowiez, Y.: Predicting preferential water flow in soils by traveling-dispersive waves, J. Hydrol., 278, 64–75, 2003.

Ellenberg, H. and Klötzli F.: Waldgesellschaften und Waldstandorte der Schweiz, Mitteilungen EAFV, 48, 587–930, 1972.
Engler, A.: Untersuchungen über den Einfluss des Waldes auf den Stand der Gewässer, Mitteilungen der Schweizerischen Zentralanstalt für das forstliche Versuchswesen, XII Band, 1919.
FAO-Unesco: Soil map of the world, ISRIC, Wageningen, 1994.
Federal Office for the Environment (FOEN): http://www.hydrodaten.admin.ch/d/2179.htm, last access: 16 May 2008.
Flury, M., Flühler, H., Jury, W. A., and Leuenberger, J.: Susceptibility of soils to preferential flow of water: A field study, Water Resour. Res., 30, 1945–1954, 1994.
Gärdenäs, A. I., Šimůnek, J., Jarvis, N., and van Genuchten, M. T.: Two-dimensional modelling of preferential water flow and pesticide transport from a tile-drained field, J. Hydrol., 329, 647–660, 2006.
Gerke, H. H.: Preferential flow descriptions for structured soils, J. Plant Nutr. Soil Sc., 169, 382–400, 2006.
Germann, P. F. and Beven, K.: Kinematic wave approximation to infiltration into soils with sorbing macropores, Water Resour. Res., 21, 990–996, 1985.
Germann, P., Helbling, A., and Vadilonga, T.: Rivulet approach to rates of preferential infiltration, Vadose Zone J., 6, 207–220, 2007.
Germann, P. F. and Hensel D.: Poiseuille flow geometry inferred from velocities of wetting fronts in soils, Vadose Zone J., 5, 867–876, 2006.
Gish, T. J., Gimenez, D., and Rawls, W. J.: Impact of roots on ground water quality, Plant Soil, 200, 47–54, 1998.
Hagedorn, F. and Bundt, M.: The age of preferential flow paths, Geoderma, 108, 119–132, 2002.
Jørgensen, P. R., Hoffmann, M., Kistrup, J. P., Bryde, C., Bossi, R., and Villholth, K. G.: Preferential flow and pesticide transport in a clay-rich till: Field, laboratory, and modeling analysis, Water Resour. Res., 38, No. 11, 1246, doi:10.1029/2001WR000494, 2002.
Kawamoto, K., Mashino, S., Oda, M., and Miyazaki, T.: Moisture structures of laterally expanding fingering flows in sandy soils, Geoderma, 119, 197–217, 2004.
Kung, K.-J. S.: Preferential flow in a sandy vadose zone: 2. Mechanism and implications, Geoderma, 46, 59–71, 1990.
Li, Y. and Ghodrati, M.: Preferential transport of nitrate through soil columns containing root

channels, Soil Sci. Soc. Am. J., 58, 653–659, 1994.
Mapa, R. B.: Effect of reforestation using *Tectona grandis* on infiltration and soil water retention, Forest Ecol. Manag., 77, 119–125, 1995.
Mitchell, A. R., Ellsworth, T. R., and Meek, B. D.: Effect of root systems on preferential flow in swelling soil, Commun. Soil Sci. Plan., 26(15, 16), 2655–2666, 1995.
Noguchi, S., Tsuboyama, Y., Sidle, R. C., and Hosoda, I.: Spatially distributed morphological characteristics of macropores in forest soils of Hitachi Ohta Experimental Watersheds, J. For. Res., 2, 207–215, 1997.
Perillo, C. A., Gupta, S. C., Nater, E. A., and Moncrief, J. F.: Prevalence and initiation of preferential flow paths in a sandy loam with argillic horizon, Geoderma, 89, 307–331, 1999.
Roth, K., Schulin, R., Flühler, H., and Attinger, W.: Calibration of time domain reflectrometry for water content measurements using a composite dielectric approach, Water Resour. Res., 26, 2267–2274, 1990.
Soil survey division staff: Soil survey manual, Soil Conservation Service, US Department of Agriculture, Handbook 18, 1993.
Tremblay, Y., Rousseau, A. N., Plamondon, A. P., Lévesque, D., and Jutras, S.: Rainfall peak flow response to clearcutting 50% of three small watersheds in a boreal forest, Montmorency Forest, Québec, J. Hydrol., 352, 67–76, 2008.
Wang, Z., Wu, Q. J., Wu, L., Ritsema, C. J., Dekker, L. W., and Feyen, J.: Effects of soil water repellency on infiltration rate and flow instability, J. Hydrol., 231–232, 265–276, 2000.
Weiler, M. and Naef, F.: An experimental tracer study of the role of macropores in infiltration in grassland soils, Hydrol. Process., 17, 477–493, 2003.
Withington, J. M., Reich, P. B., Oleksyn, J., and Eissenstat, D. M.: Comparisons of structure and life span in roots and leaves among temperate trees, Ecol. Monogr., 76(3), 381–397, 2006.

Table 1. Characteristics of the irrigated plots.

Site	Tree diameter cm	Distance to stem m	Soil type[1]	pH $CaCl_2$ (range)		Texture[2]		Average bulk density Mg m^{-3}		Average Porosity m^3 m^{-3}	
				T	*S*	*T*	*S*	*T*	*S*	*T*	*S*
Spruce 1	60	1	Gleyic Cambisol	6.2–6.3	6.2–6.9	Clay loam	Clay loam	0.85	1.25	0.68	0.53
Spruce 2	80	3.7	Mollic Gley	6.2	6.17–7.35	Clay loam	Clay loam	0.73	1.31	0.72	0.51
Spruce 3	7	1	Mollic Gley	3.0–3.2	3.3–4.1	Sandy loam	Loam	0.99	1.35	0.63	0.49
Fir 1	65	1	Gleyic Cambisol	3.1–3.8	3.4–6.1	Sandy clay loam	Clay loam	0.19	1.35	0.92	0.49
Fir 2	33	1	Gleyic Cambisol	3.4	3.6–6.2	Sandy loam	Loam	0.88	1.43	0.67	0.46
Fir 3	35	1	Eutric Cambisol	2.9–3.6	3.3–3.7	Sandy loam	Clay loam	0.94	1.29	0.65	0.51
Fir 4	65	3.2	Mollic Gley	6.6	6.4–7.4	Loam	Clay loam	0.70	1.34	0.73	0.49
Fir 5	18	1	Mollic Gley	2.8–3.1	3.1–7.5	Sandy clay loam	Loam	0.63	1.38	0.76	0.48
Beech 1	40	1	Gleyic Cambisol	2.9–3.4	3.5–6.2	Sandy clay loam	Sandy clay loam	0.62	1.42	0.76	0.46
Beech 2	40	1	Gleyic Cambisol	2.9–3.4	3.5–6.2	Sandy clay loam	Sandy clay loam	0.62	1.42	0.76	0.46
Beech 3	46	3.5	Mollic Gley	6.4	6.7–7.4	Clay loam	Clay	0.72	1.26	0.73	0.52
Beech 4	13	1.5	Stagnic Cambisol	3.1–3.5	3.3–3.8	Sandy loam	Clay loam	1.01	1.21	0.61	0.54
Beech 5	3	1	Gleyic Cambisol	3.0–3.8	3.5–4.8	Sandy loam	Clay loam	0.75	1.30	0.71	0.51

[1]: FAO-Unesco (1994).
[2]: Soil survey division staff (1993).
T: topsoil.
S: subsoil.

Table 2. Key points in the measured time series of preferential infiltration.

ID#	Site	Depth of TDR m	θ_{in} m^3 m^{-3}	θ_{max} m^3 m^{-3}	θ_F m^3 m^{-3}	w_s m^3 m^{-3}	q 10^{-6} m s^{-1}	v_w mm s^{-1}	L 10^3 m m^{-2}	F μm
1	Spruce 1	0.12	0.301	0.424	0.321	0.103	12.88	0.22	12.982	6.5
2	Spruce 2	0.05	0.473	0.546	0.465	0.081	19.24	0.83	8.072	10.4
3	Spruce 3	0.05	0.369	0.506	0.369	0.137	14.42	0.41	15.683	7.2
4	Spruce 3	0.2	0.443	0.526	0.442	0.084	31.01	1.11	5.342	14.0
5	Fir 1	0.04	0.244	0.372	0.245	0.127	12.09	0.17	24.489	4.5
6	Fir 1	0.24	0.388	0.441	0.389	0.052	18.01	0.8	3.508	12.4
7	Fir 1	0.45	0.359	0.388	0.366	0.022	6.36	0.47	1.846	11.9
8	Fir 2	0.04	0.408	0.467	0.419	0.048	3.05	0.17	9.647	4.2
9	Fir 2	0.17	0.406	0.444	0.413	0.031	11.74	0.57	2.546	10.7
10	Fir 3	0.26	0.357	0.404	0.373	0.031	3.44	0.18	3.837	8.0
11	Fir 3	0.42	0.442	0.504	0.448	0.056	31.8	10	3.251	18.1
12	Fir 4	0.06	0.445	0.583	0.446	0.137	18.69	a)	18.922	6.1
13	Fir 5	0.17	0.471	0.56	0.508	0.052	4.16	0.11	6.034	7.2
14	Fir 5	0.23	0.501	0.55	0.499	0.051	14.33	0.95	4.163	12.8
15	Beech 1	0.05	0.295	0.424	0.293	0.131	9.12	0.17	18.579	5.7
16	Beech 1	0.18	0.427	0.482	0.427	0.055	9.45	0.25	4.831	10.5
17	Beech 2	0.08	0.428	0.52	0.434	0.086	1.69	0.66	9.102	9.2
18	Beech 2	0.18	0.432	0.473	0.438	0.035	4.46	0.15	3.166	9.1
19	Beech 3	0.04	0.451	0.599	0.456	0.143	19.9	a)	25.116	4.8
20	Beech 4	0.65	0.371	0.413	0.385	0.028	9.04	0.43	1.905	14.0
21	Beech 5	0.45	0.477	0.503	0.482	0.021	8.01	0.68	1.448	13.6

Depth of TDR: position of TDR-probe beneath soil surface.
θ_{in}: initial volumetric soil moisture.
θ_{max}: maximum volumetric soil moisture.
θ_F: volumetric water content after a drainage of 20 h.
w_s: difference between θ_{max} and θ_F.
q: volume flux density.
v_w: average velocity of wetting front.
L: maximal sum of contact lengths between the mobile water and soil for $\theta_{(Z,t)} \geq \theta_F$.
F: arithmetic mean of film thickness of mobile water for $\theta_{(Z,t)} \geq \theta_F$.
a): No data available as t_w=0.

Table 3. Matrix of Pearson product-moment correlation coefficients among water-flow determinants and fine root parameters.

	Depth	θ_{in}	θ_{max}	θ_F	w_s	v_w^1	q	L	F	FRL	FRA	FRV	BD
Depth	1.000												
θ_{in}	0.113	1.000											
θ_{max}	−0.304	0.813***	1.000										
θ_F	0.143	0.989***	0.796***	1.000									
w_s	−0.697***	−0.298	0.297	−0.342	1.000								
v_w^1	0.196	0.544*	0.484*	0.469*	−0.116	1.000							
q	0.107	0.128	0.166	0.068	0.150	0.736***	1.000						
L	−0.689***	−0.403	0.160	−0.429	0.925***	−0.397	−0.100	1.000					
F	0.757***	0.416	0.027	0.389	−0.571**	0.787***	0.567**	−0.745***	1.000				
FRL	−0.715***	−0.305	0.166	−0.332	0.781***	−0.442	−0.174	0.868***	−0.775***	1.000			
FRA	−0.673**	−0.277	0.220	−0.311	0.832***	−0.421	−0.102	0.915***	−0.725***	0.953***	1.000		
FRV	−0.632**	−0.290	0.192	−0.328	0.816***	−0.371	−0.028	0.899***	−0.671**	0.870***	0.973***	1.000	
BD	0.711***	0.133	−0.300	0.123	−0.659**	0.451	0.329	−0.738***	0.738***	−0.684**	−0.689***	−0.680**	1.000

Depth: position of TDR-probe beneath soil surface.
θ_{in}: initial volumetric soil moisture.
θ_{max}: maximum volumetric soil moisture.
θ_F: volumetric water content after a drainage of 20 h.
w_s: difference between θ_{max} and θ_F.
v_w: average velocity of wetting front.
q: volume flux density.
L: maximum sum of contact lengths between the mobile water and soil.
F: arithmetic mean of film thickness of mobile water.
FRL, FRA, FRV: length, surface area and volume of fine roots per soil volume.
BD: Bulk density.
*P<0.05, **P<0.01, ***P<0.001, no appendix: not significant.
[1]Only 19 horizons were considered as t_w=0 in two cases.

Table 4. Components of water flow of the modelled water content waves.

Fine root density cm cm^{-3}	L m m^{-2}	F μm	w_s m^3 m^{-3}	v_W m m s^{-1}	q 10^{-6} m s^{-1}
0.25	4543	11.5	0.050	0.43	22.4
0.5	7407	10.2	0.072	0.34	25.8
1	13 134	7.7	0.095	0.19	19.4
1.5	18 861	5.2	0.089	0.09	8.5
1.75	21 725	3.9	0.075	0.05	4.2

L: maximum sum of contact lengths between mobile water and soil.
F: arithmetic mean of film thickness of mobile water.
w_s: decrease in soil moisture during a 20 h drainage.
v_w: average velocity of wetting front.
q: volume flux density.

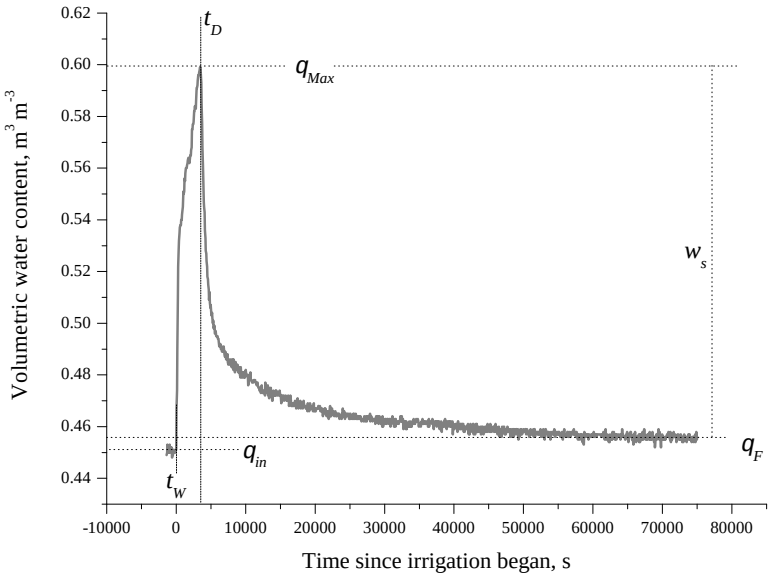

Fig. 1. Definitions of parameters and variables of a water content wave (wcw), shown for ID# 19 (according to Table 2), depth 0.04 m. t_W: arrival of first measurable moisture increase; t_D: arrival time of drainage front; θ_{in}: initial volumetric soil moisture; θ_{max}: maximum volumetric soil moisture; θ_F: final volumetric soil moisture after a drainage of 20 h; w_s: $\theta_{max}-\theta_F$, amplitude of moisture wave.

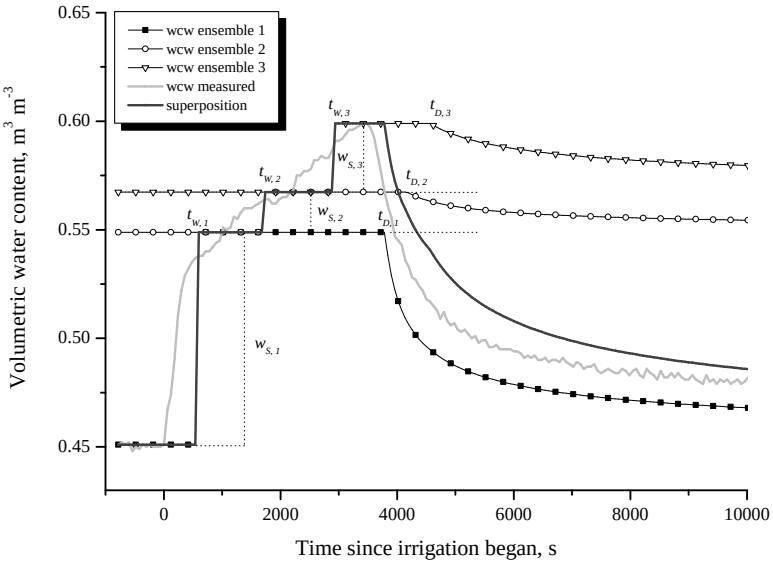

Fig. 2. Superposition of three rivulet ensembles applied to data of ID# 19 (according to Table 2). wcw: water content wave; $t_{W,j}$: arrival time of first measurable moisture increase in the jth rivulet ensemble; $t_{D,j}$: arrival time of drainage front of the jth rivulet ensemble; $w_{s,j}$: amplitude of moisture wave of the jth rivulet ensemble.

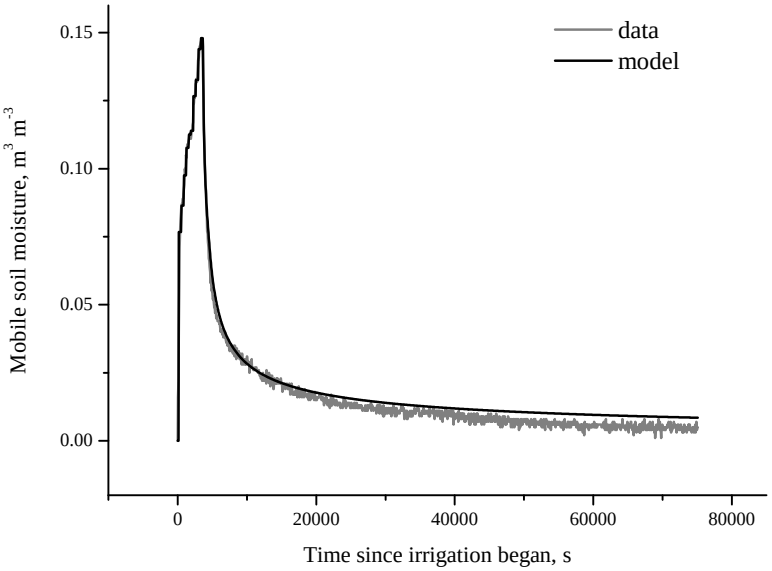

Fig. 3. Ten rivulet ensembles applied to data of the third irrigation of ID# 19 (according to Table 2) at a depth of 0.04 m. Comparison of superimposed trailing wave with measured data.

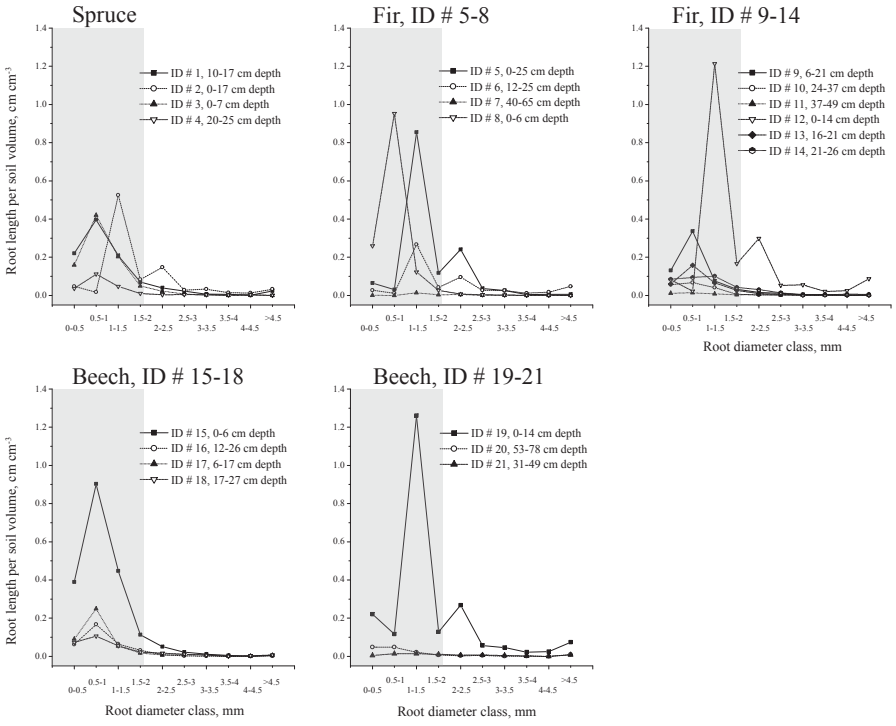

Fig. 4. Root length per soil volume of varying root diameter classes of the horizons where volumetric water content was measured. Depth in the legend refers to the depths where roots were separated. Grey shaded area: fine roots (diameter≤2 mm). ID# according to Table 2. To improve readability, the root lengths of trees at the fir and beech sites are shown separately in two different graphs.

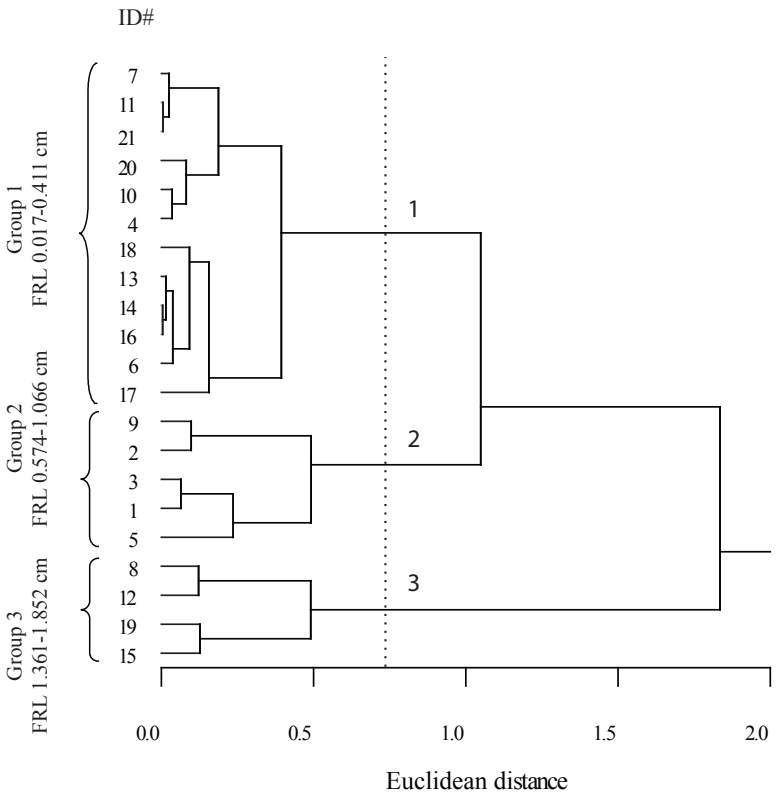

Fig. 5. Cluster analysis of fine root length per soil volume (FRL) of the 21 layers where the wave-guides were installed (ID# according to Table 2). Dashed line: Euclidean distance that separates the three FRL groups.

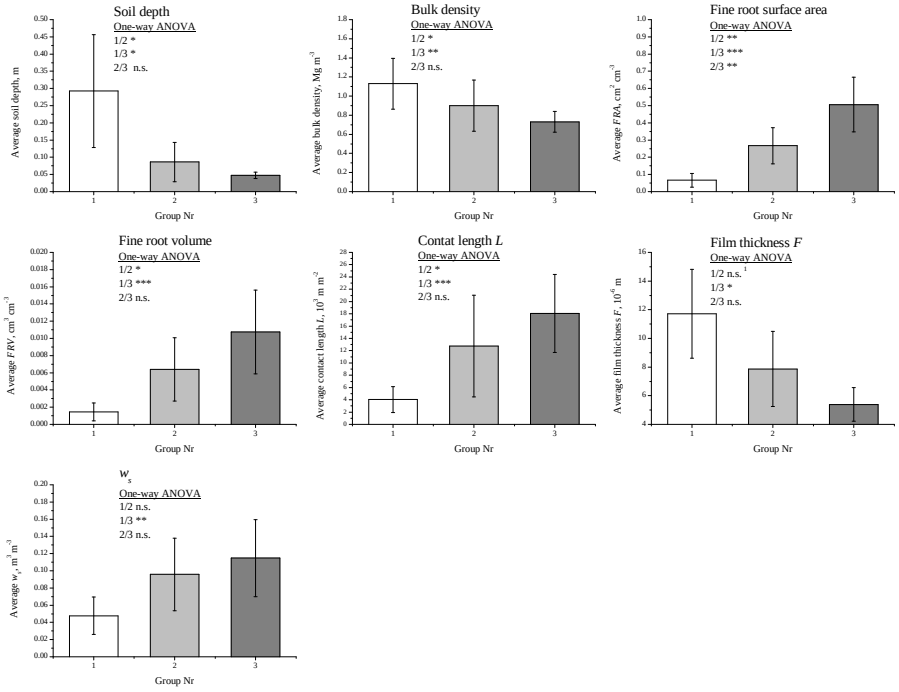

Fig. 6. Soil, root and preferential flow parameters of the three fine root length groups. White column: group 1 (FRL 0.017–0–411 cm cm^{-3}), grey column: group 2 (FRL 0.574–1.066 cm cm^{-3}), dark grey column: group 3 (FRL 1.361–1.852 cm cm^{-3}). Probability levels for the one-way ANOVA: $^{*}P<0.05$, $^{**}P<0.01$, $^{***}P<0.001$, n.s.: not significant. [1]significant at $P<0.1$. Bars indicate standard error.

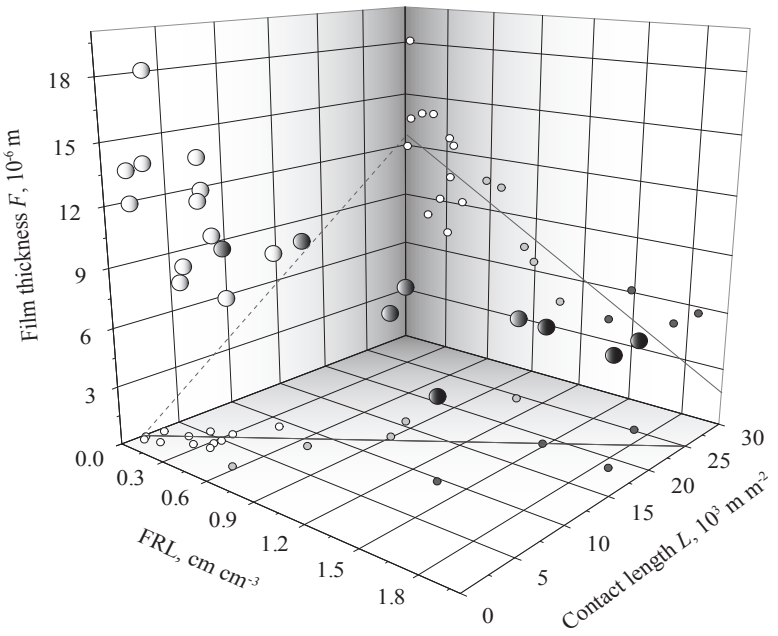

Fig. 7. Relationship between fine root length per soil volume FRL, maximum sum of contact lengths L and arithmetic mean of film thickness F of mobile water. Large balls: data points in XZY-space; small circles: data projections on XY- and XZ-plane. White: FRL-group 1, grey: FRL-group 2, dark grey: FRL-group 3 (Fig. 5). Grey lines: linear correlation between fine root length FRL and contact length L (L = 11.454 FRL + 1.6794), fine root length FRL and film thickness F (F = −5.3893 FRL + 12.561). Dashed grey line: cutting line of the regression plane and the YZ-plane.

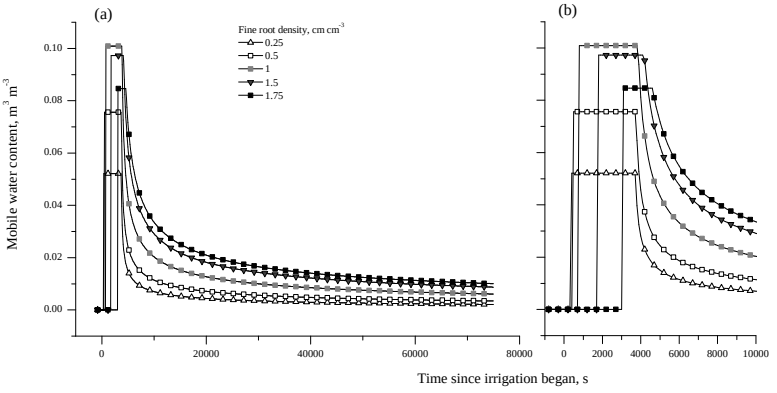

Fig. 8. Modelled water content waves of different fine root densities at a depth of 15 cm. **(a)**: 1 h irrigation and subsequent drainage, **(b)**: first 10 000 s of the irrigation and subsequent drainage. Duration of irrigation: 3600 s, starting at t = 0.

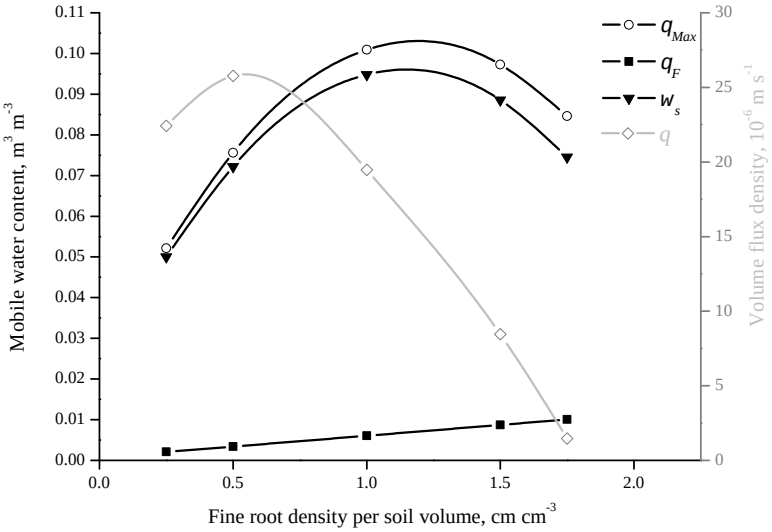

Fig. 9. Hydrological properties of modelled trailing waves with different root densities. θ_{max}: maximum volumetric soil moisture; θ_F: volumetric water content after a drainage of 20 h; w_s: difference between θ_{max} and θ_F; q: volume flux density.